View metadata, citation and similar papers at core.ac.uk
brought to you by CORE
provided by NASA Technical Reports Server

IAC-05-D2.6.01

X-43A HYPERSONIC VEHICLE TECHNOLOGY DEVELOPMENT

Randall T. Voland
Lawrence D. Huebner
Charles R. McClinton (retired)
NASA Langley Research Center, Hampton, VA, USA

ABSTRACT

NASA recently completed two major programs in Hypersonics: Hyper-X, with the record-breaking flights of the X-43A, and the Next Generation Launch Technology (NGLT) Program. The X-43A flights, the culmination of the Hyper-X Program, were the first-ever examples of a scramjet engine propelling a hypersonic vehicle and provided unique, convincing, detailed flight data required to validate the design tools needed for design and development of future operational hypersonic airbreathing vehicles. Concurrent with Hyper-X, NASA's NGLT Program focused on technologies needed for future revolutionary launch vehicles. The NGLT was "competed" by NASA in response to the President's redirection of the agency to space exploration, after making significant progress towards maturing technologies required to enable airbreathing hypersonic launch vehicles. NGLT quantified the benefits, identified technology needs, developed airframe and propulsion technology, chartered a broad University base, and developed detailed plans to mature and validate hypersonic airbreathing technology for space access. NASA is currently in the process of defining plans for a new Hypersonic Technology Program. Details of that plan are not currently available. This paper highlights results from the successful Mach 7 and 10 flights of the X-43A, and the current state of hypersonic technology.

INTRODUCTION

H. Julian Allen made an important observation in the 1958 25th Wright Brothers Lecture: "Progress in aeronautics has been brought about more by revolutionary than evolutionary changes in methods of propulsion."[1] Steam engines replaced sails and introduced mass transportation on the sea and lead to the railroads. The internal combustion engine replaced the horse for private transportation and lead to the airplane. The jet engine replaced the piston engine, and revolutionized the airliner, taking it routinely above the weather and beyond the seas. Modern rockets opened the space age for the bold and wealthy. In the 21st century, revolutionary applications of airbreathing propulsion will make space travel routine and intercontinental travel as easy as intercity travel today. One of NASA's focuses today remains the application of revolutionary propulsion systems for space transportation.

Figure 1 represents the first application of this revolutionary propulsion technology to space access missions with an airline-sized space vehicle that serves as a high-speed, high-altitude, first-stage launch platform for an expendable or reusable rocket-powered second stage[2]. This modest approach significantly improves launch safety and reliability. In addition, it places the world on a new path to reduced cost for space access which cannot be achieved with evolutionary improvements of current systems.

Benefits of airbreathing launch systems are safety, mission flexibility, robustness, and operating costs[2] as highlighted in figure 2. Safety benefits result from characteristics such as abort capability and power density. Horizontal takeoff and powered landing allows ability to abort over most of the flight, both ascent and decent. High lift-to-drag ratio (L/D) allows longer-range glide for a large landing footprint. Power density, or the quantity of propellant pumped, is 1/10 that of a vertical take off rocket due to lower thrust loading (T/W), smaller vehicle weight and higher specific impulse (Isp), defined as thrust per pound of propellant—a measure of efficiency. Power density is a large factor in catastrophic failures. Recent analysis indicates that safety increases by several orders of magnitude are possible using airbreathing systems. Mission flexibility results from horizontal takeoff and landing, the large landing (unpowered) footprint and high L/D. Utilization of aerodynamic forces rather than thrust allows efficient orbital plane changes during ascent, and a wider launch window. Robustness and reliability can be built into airbreathing systems because of large margins and reduced weight-growth sensitivity, and the low thrust required for smaller, horizontal takeoff systems. Cost models under development for airbreathing launch systems indicate about one order-of-magnitude reduction in operating cost is possible.

The development of reusable launch vehicles holds great promise as the key to unlocking the vast potential

of space for business exploitation. Only when access to space is assured in a system that provides routine operation with airline-like safety and affordable cost will businesses be willing to take the risks and make the investments necessary to realize this great potential. Rocket-powered vehicles are approaching their limits in terms of these parameters[2]; switching to a new approach is the only way to achieve significant improvements. Airbreathing vehicles that are capable of hypersonic speeds can transform access to space, just like turbojets transformed the airline business.

Figure 1. Revolutionary Launch Vehicle

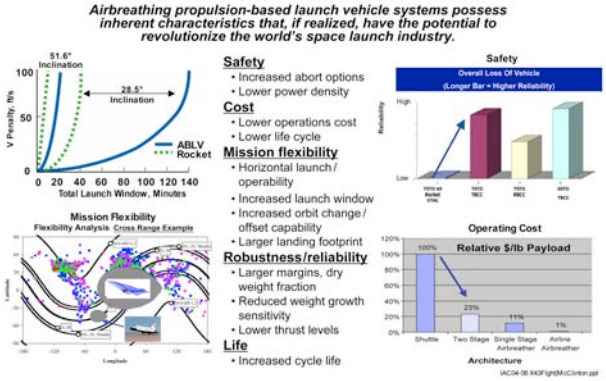

Figure 2. Benefits of Hypersonic Airbreathing Vehicles

NASA has funded hypersonic vehicle and propulsion technology for over 40 years, aiming at futuristic space launch capabilities[3]. This work represents the next frontier in air vehicle design. Recent U.S. industry focus has been on avionics, stealth, and methods of making the last generation of aircraft more effective. Evolutionary vehicle changes will give way to revolutionary changes when a new propulsion system is available. Studies by the Next Generation Launch Technology (NGLT) Program reconfirmed that hypersonic systems using turbine-based "low-speed" engines combined with scramjets for higher speed operation, up to at least Mach 7 and eventually to Mach 13-15, are the preferred long-term approach for airbreathing space access vehicles. Clearly, these turbine-based systems are also needed for super-sonic cruise/hypersonic dash or pure hypersonic cruise aircraft of the future (fig. 3).

Figure 3. Future Hypersonic Air Vehicles

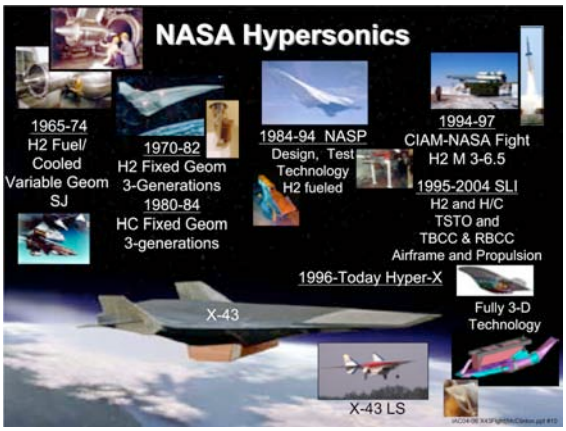

Figure 4. Historical Perspective

NASA funded scramjet technology development, focused mostly on the propulsion cycle efficiency with numerous ground tests in wind tunnels (fig. 4) over the past 40 years[3]. Starting in the mid 1960's, NASA built and tested a hydrogen-fueled and -cooled scramjet engine that verified scramjet cycle efficiency, structural integrity, first-generation design tools, and engine system integration. Starting in the early 1970's, NASA designed and demonstrated a fixed-geometry, airframe-integrated scramjet "flowpath" capable of propelling a hypersonic vehicle from Mach 4 to 7 in wind tunnel tests. Starting in the mid 1980's, NASA teamed with the Department of Defense in the National AeroSpace Plane (NASP) Program to demonstrate hypersonic technologies required for a hypersonic, scramjet-based, combined-cycle powered, single-stage-to-orbit launch vehicle. Under the NASP program NASA focused on engine definition and testing for both the aerodynamic lines/cycle efficiency and hydrogen-cooled engine structure.

NASA developed the concept for the Hyper-X (X-43A) Program in 1995-1996 as a result of several blue-ribbon panel recommendations that flight experiments of airframe-integrated scramjet-propulsion systems be the next major step in hypersonic research. The experts agreed that, at a minimum and as a first step, a vehicle must fly with an airframe-integrated supersonic-combustion ramjet (scramjet) propulsion system. Consequently NASA initiated the Hyper-X

program[1] to provide the flight data to validate the design tools and methods to be used in the development of future hypersonic vehicles. The program goals were established to provide performance data to reduce development risks for subsequent, operational vehicles; to advance performance-prediction capabilities for airbreathing hypersonic vehicles; to flight-validate airframe-integrated scramjet performance and design methods; and to flight-validate other selected, key technologies.

The Hyper-X team developed the X-43A as a small-scale research vehicle to provide flight data for a hydrogen-fueled, airframe-integrated scramjet engine[4]. In addition, aerodynamic, thermal, structural, guidance, flush-air-data-system, and other data were to be obtained. Test plans called for boosting each of three X-43A research vehicles to the required test condition by a drop-away booster. The resulting 12' long vehicle is illustrated in figure 5. The development of the X-43A and its systems are detailed in references 5-13.

The NASA Hyper-X program employed a low-cost approach to design, build, and flight test three small, airframe-integrated scramjet-powered research vehicles at Mach 7 and 10. The research vehicles were dropped from the NASA Dryden B-52, rocket-boosted to test point by a modified Pegasus first stage, separated from the booster, and then operated in autonomous flight. Tests were conducted at approximately 100,000 ft. at a dynamic pressure of about 1000 psf.

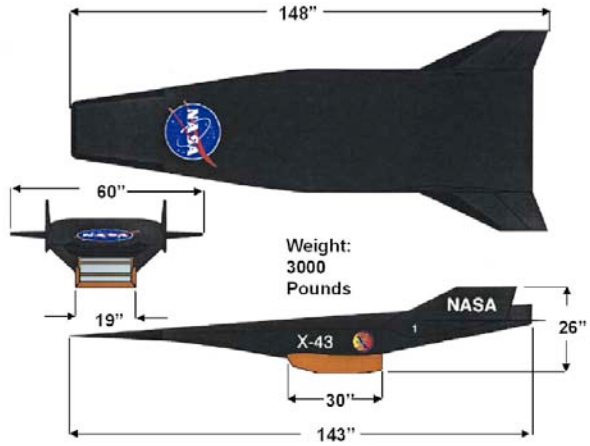

Figure 5. X-43A Vehicle Geometry

FLIGHT RESULTS

The first Mach 7 flight was attempted June 2, 2001. This flight failed when the launch vehicle went out of control early in the flight. The second flight occurred March 27, 2004. The flight was completely successful, and demonstrated acceleration of the X-43A vehicle during climbing flight at Mach 6.83. Preparations for the third flight started before the second flight was completed. The third flight occurred November 16, 2004. This final flight successfully demonstrated cruise thrust at Mach 9.68. Many technical results from these flights will be discussed herein. Details on the preparation and execution of these flights are addressed in references 14-17.

The second flight trajectory is illustrated in figure 6. The launch vehicle was dropped from the B-52 flying at Mach 0.8 and 40,000 feet. The booster ignited after 5-seconds free fall to about 39,500 feet. The launch vehicle executed a 1.9g pull-up, followed by a 0.7g pushover to achieve nearly level flight at 95,000 ft. Following burnout and stage separation, the engine opened for about 30 seconds: 5 seconds of fuel-off tare, 11 seconds of powered flight (at about Mach 6.83 and dynamic pressure of 980 psf), another 5 seconds of unpowered steady tare, followed by 10 seconds of parameter identification (PID) maneuvers[18]. The engine cowl then closed, and the vehicle flew a controlled descent over 300 NM to “splash-down” in the Pacific Ocean. The powered portion of this flight included 1.5 seconds for ignition, followed by hydrogen fuel ramp up and ramp down[19] to generate a large database.

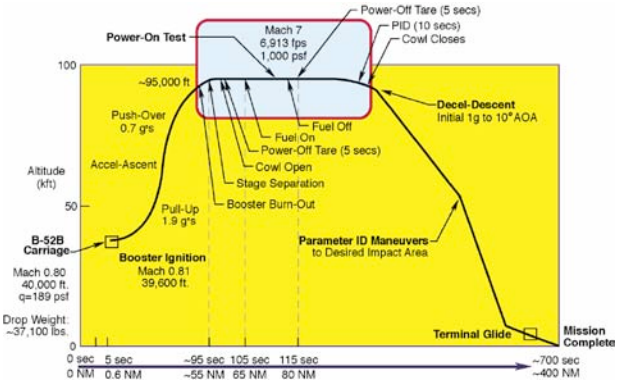

Figure 6. Flight 2 Trajectory

The flight 3 trajectory was somewhat different than flight 2. The B-52 flight conditions were the same; however, the launch vehicle executed a 2.5g pull-up to a flight path angle of over 30 degrees, followed by 0.5g push over to achieve nearly level flight at 110,000 ft. Following burnout and stage separation, the engine opened for about 20 seconds: 3 seconds of fuel-off tare, 11 seconds of powered flight (at about Mach 9.68 and dynamic pressure of 930 psf), and another 6 seconds of unpowered steady tare. (No cowl-open PID maneuvers were performed due to cowl survival concerns.) The engine cowl closed, and the vehicle flew a controlled descent over 800NM to “splash-down” in the Pacific Ocean. During descent, PID maneuvers were successfully performed at each successively decreasing Mach number[18]. The powered portion of flight included 5 seconds of silane-piloted operation at two fuel equivalence ratio settings, followed by hydrogen-only fueled operation at two settings, then ramp down[19]. This conservative approach assured good data before trying to operate the small engine without piloted fuel.

The following discussion highlights flight 2 and flight 3 data and results from design tool validation studies. The flight results contain much commonality, so the results are presented in terms of flight sequence and technology areas, including results from both successful flights. These are designated as F2 for the successful 2nd flight that targeted Mach 7, and F3 for the 3rd flight that targeted Mach 10.

EXPERIMENTAL MEASUREMENTS

The X-43A vehicles were well instrumented, with over 200 measurements of surface pressure; over 100 thermocouples to measure surface, structure and environmental temperatures; and discrete local strain measurements on the hot wings and tail structure. The flight management unit included a highly accurate 3-axis measurement of acceleration and rates. In addition, over 500 data words were extracted from the flight computer. Instrumentation density is illustrated in figure 7 by external and internal wall pressure and temperature on the lower body surface. Internal engine instrumentation on the body side is more dense in order to capture internal flow details of the engine.

All of the data from the X-43A flights were successfully telemetered and captured by multiple air and ground stations. The instrumentation health and performance were excellent: very few lost instruments/parameters, extremely low noise content, no significant calibration issues, no significant delay or time-lag issues, and extremely limited TM drop outs. Accuracy of these measurements benefited from day-of-flight atmospheric measurements by weather balloons. These measurements provide a small change in flight Mach number and dynamic pressure vis-à-vis atmospheric conditions and winds from historical atmospheric tables. Flight 2 Best Estimated Trajectory (BET) resulted in higher dynamic pressure and Mach number, but only a trivial change in angle of attack (AOA). Flight 3 BET resulted in lower dynamic pressure and higher Mach number and AOA. The flight trajectory reconstruction is discussed in reference 22.

The data obtained from these flights meets the primary Hyper-X Program objective: validation of design methods including experimental, analytical and computational methods. The data was released to the US hypersonic community in the form of complete classified data packages[20,21] to more than 20 US Government and industrial entities and well over 50 classified and unclassified papers and presentations.

X-43A Free Flight

Following stage separation from the rocket booster (boost and stage separation discussed in references 23-27), the X-43A F2 research vehicle stabilized to 2.5° AOA, and the engine cowl was opened. After 5 seconds of tare force measurements, the engine was ignited with a pyrophoric silane-hydrogen fuel mixture (left side of fig. 8), then switched to pure hydrogen fuel for about 10 seconds of powered flight. The contrail from the pure-hydrogen fuel was not visible in the raw image from the High-Altitude Observatory (HALO) aircraft (right side of fig. 8).

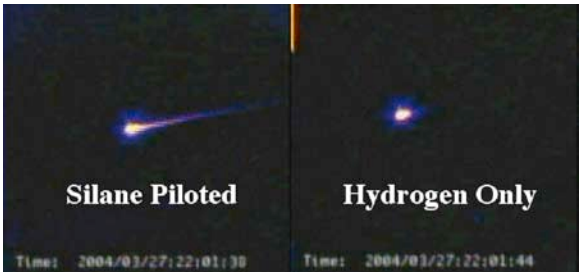

Figure 8. X-43A Powered Flight Video From Army HALO Aircraft

Following powered flight, with the engine cowl open, the vehicle performed pre-programmed PID maneuvers to quantify the X-43A aerodynamic stability and control derivatives[18]. These maneuvers lasted 15 seconds, after which the engine cowl was closed, the vehicle glided another 300 miles, and splashed into the Pacific Ocean. During the descent of both flights, the vehicle

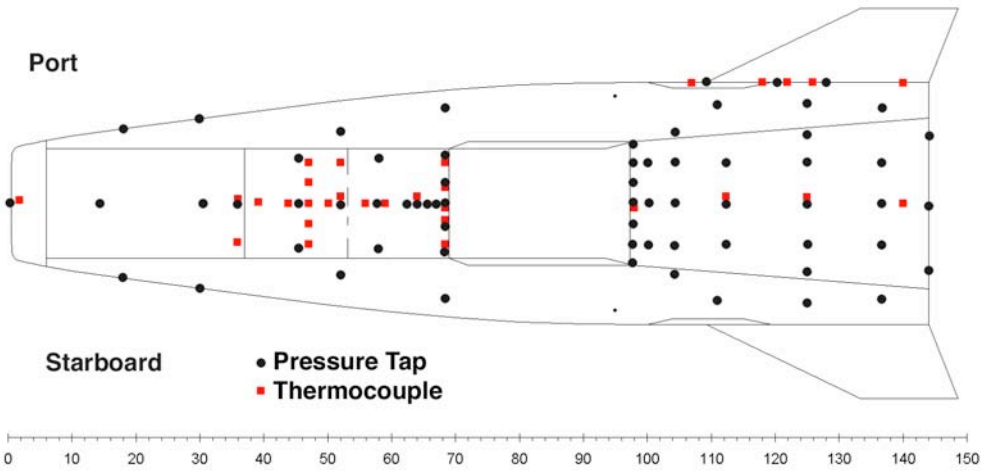

Figure 7. Lower Surface Instrumentation

continued to perform a series of PID maneuvers at each decreasing Mach number to Mach 2. This segment of the flight provided a large, unique aerodynamic database for sharp leading edge lifting body configurations that will be used to validate wind tunnel data and computational tools.

Scramjet Powered Vehicle Performance

For Mach 7, flight 2 the X-43A was commanded to fly at 2.5 degrees angle of attack during the cowl-open portion of the flight. However, as the fuel is turned-on/off and the throttle adjusted, the pitching moment changes significantly. Figure 9 illustrates the measured angle of attack—from cowl open to fuel off and the start of the Mach 7 PID maneuvers. During the scramjet-powered segment, the AOA was maintained to 2.5° ± 0.2°, except during flameout. Some efforts were made in the flight control system to provide feed-forward control. For Mach 10, flight 3, the vehicle was commanded to fly at 1.0 degree angle of attack during the cowl open segment. The vehicle maintained pitch control about the same as during the powered segment of F2.

For both F2 and F3 the fuel sequencing for powered flight starts with a silane/hydrogen mixture to assure ignition, then transitions to pure hydrogen fuel. The ignition sequence for F2 requires about 1.5 seconds. With transition to pure hydrogen fuel, the throttle is ramped up to either a predetermined or controlled maximum value, and then decreased as the fuel is depleted from the tanks. The resulting vehicle performance is characterized by vehicle acceleration, as shown in figure 9. The ignition sequence for F3 was different—the silane remains on for the first two fueled conditions, requiring 5 seconds of piloted data. Then the same equivalence ratio test conditions were run with only hydrogen.

The green band in figure 9 illustrates pretest Monte Carlo predictions of acceleration (using an unclassified representative propulsion database). The heavy blue line depicts flight data trends. The vehicle deceleration is greater than predicted, both with cowl closed and open[28] because of two factors: 1) actual flight conditions vs predicted (2/3 of the error), and 2) vehicle drag is higher than predicted (1/3 of the error). However, the drag was within the uncertainty associated with the wind tunnel database[30, pg. 831]. The uncertainty was not resolved/reduced before flight because it did not threaten the outcome of the engine tests. Flight data will be used to help resolve the wind tunnel uncertainty for future flights/missions.

Under scramjet power the F2 vehicle acceleration was positive, and varies with throttle position. The increment in acceleration is about as predicted, which confirms the predicted engine thrust to within less than 2%[5]. It should be noted that the engine throttle was varied over a wide range without engine unstart or flame-out. Under scramjet power the F3 vehicle cruised (thrust = drag) at the reference fuel equivalence ratio with 2% silane pilot, and engine thrust was in agreement with predictions[31].

The predicted scramjet performance is also confirmed by the excellent comparison of pre-test predicted and flight scramjet flowpath wall pressure (fig. 10). Data is presented from vehicle nose to tail for F2 (fig. 10(a)), and from cowl leading edge to cowl trailing edge for F3 (fig. 10(b)). The Mach 7 data is clearly operating in "dual mode," with sonic flow in the isolator dissipating the inlet shocks. The Mach 10 data exhibits classical pure supersonic combustion mode, and the combustor pressure is shock dominated. The pretest prediction for Mach 7 was made using the SRGULL code, with

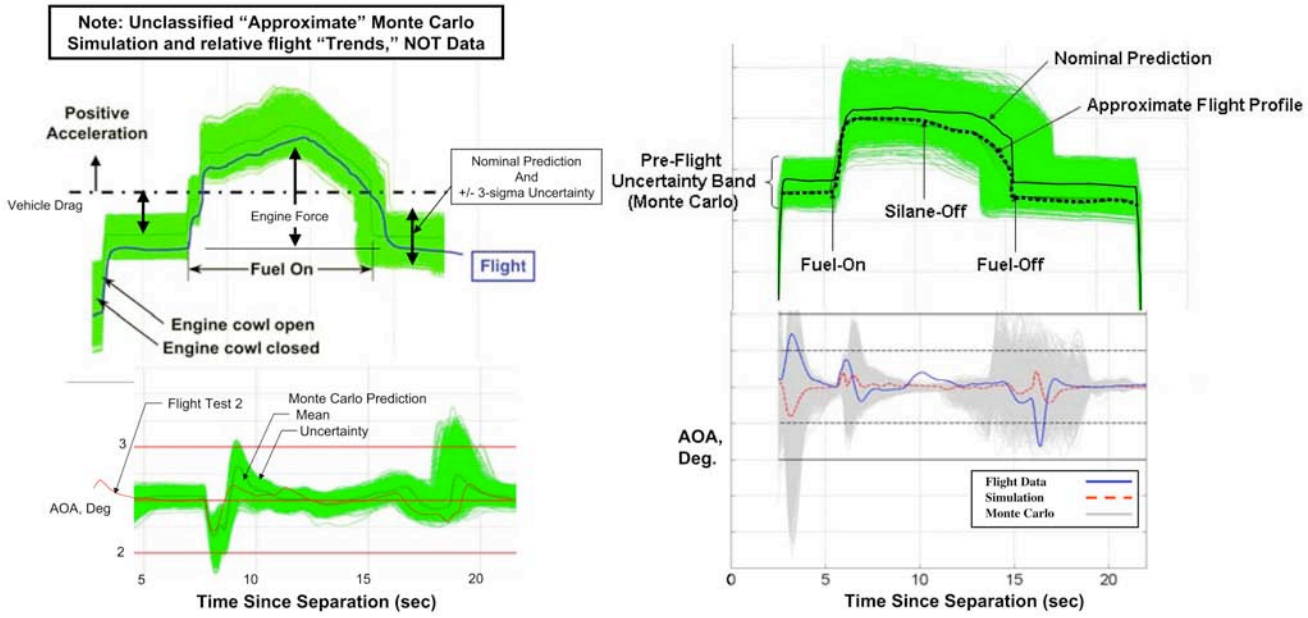

a) Flight 2, Mach 6.83 *b) Flight 3, Mach 9.68*

Figure 9. X-43A Axial Acceleration and Angle of Attack During Powered Flight

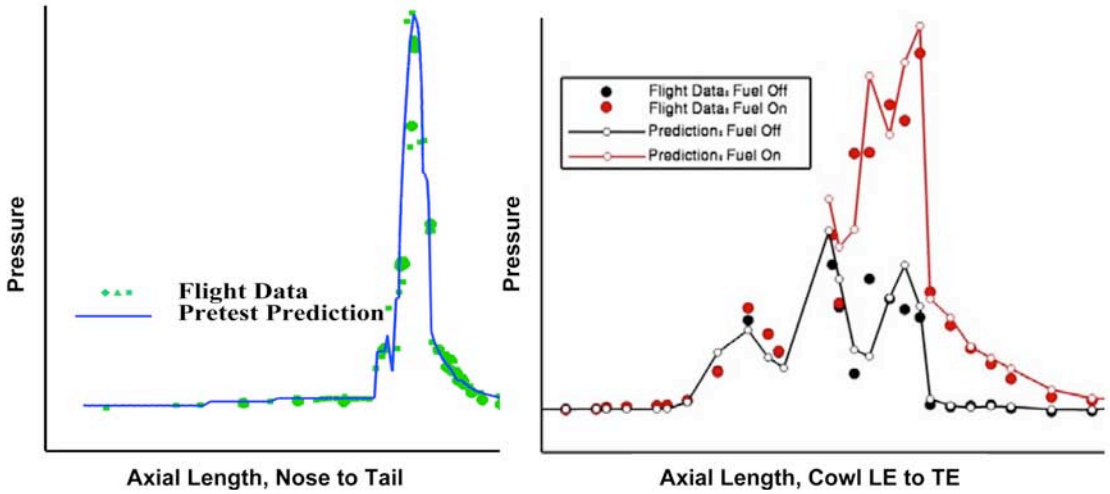

a) F2, Mach 6.83. *b) F3, Mach 9.68.*

Figure 10. X-43 Flowpath Pressure Distribution: Design Throttle Position

combustion efficiency determined by analysis of multiple wind tunnel tests, most notably, the 8-Foot High Temperature Tunnel (8-Ft. HTT) test of the Hyper-X Flight Engine (HXFE) on the Vehicle Flowpath Simulator (VFS). The Mach 10 pretest prediction was performed using a combination of CFD tools, with the SHIP code used for the combustor. The reaction efficiency used in the SHIP code was derived from analysis of data from the HYPULSE Scramjet Module test. Storch[5] and Ferlemann[31] present a detailed discussion of these codes and the pretest predictions for F2 and F3 respectively.

Wind Tunnel / Flight Scramjet Comparison

Comparison of the wall pressure measured in four wind tunnel tests with F2 data is included in references 6 and 32. Likewise, results from shock tunnel tests are compared with F3 data in reference 33. Tests with nearly identical fuel equivalence ratio were selected for comparison. Figure 11 illustrates the resulting comparison of internal wall pressure for the 8-Ft HTT test of the HXFE on the VFS and is typical of results from other wind tunnel tests. These data show that the flowfield in the isolator was separated on the cowl side, and featured a supersonic stream, evidenced by shock structure on the body side through most of the combustor length. In other words, the isolator was not "pushed" very hard for this design condition. Storch discusses the implication of this agreement, and the impact on observed combustor performance in reference 5. Rogers reported a similar trend for the Mach 10, flight 3 data[33]. These results show that ground tests are representative of flight, if careful attention is paid to modeling the appropriate flow phenomena.

Aerothermal/Thermo-Structural Analysis and Boundary Layer Transition

The design of the X-43A research vehicle structure and thermal protection system depended greatly on accurate estimation of the aerothermal environment,

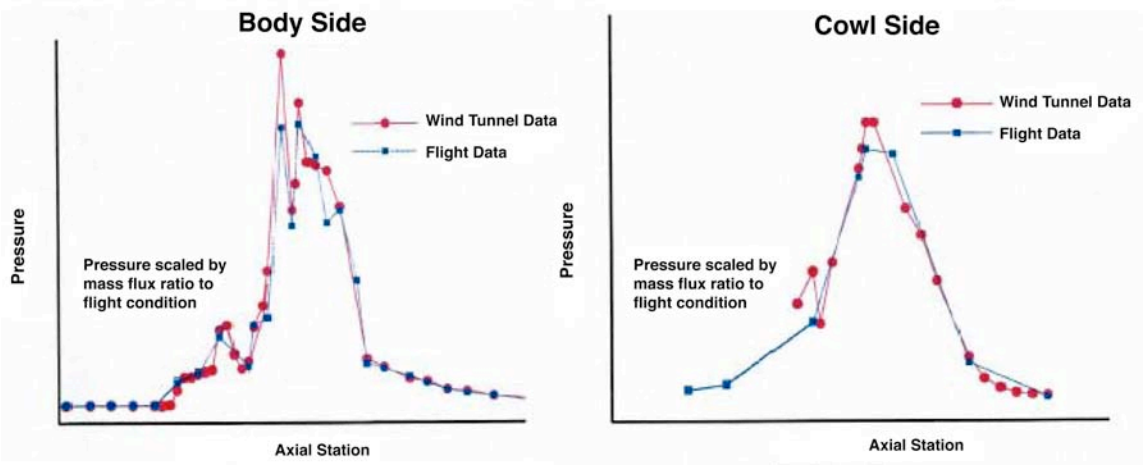

Figure 11. X-43A Flowpath Pressure Distribution Comparison With Wind Tunnel Data: Design Throttle Position

which required understanding of the boundary layer state during the entire flight. For design purposes, the lower surface flowpath into the inlet was assumed turbulent due to the inclusion of boundary layer trips near the forebody leading edge. The trips were required to insure the forebody boundary layer was turbulent for mitigation of any flow separations along the engine flowpath due to adverse pressure gradients. A substantial research and design effort was executed to ensure proper sizing of the trips with minimum induced trip drag[30, pg. 853]. The upper surface, however, was predicted to be laminar during the Mach 7 test point, based on a pre-flight trajectory using a classical correlation methodology (momentum thickness Reynolds number over Mach number of 305).

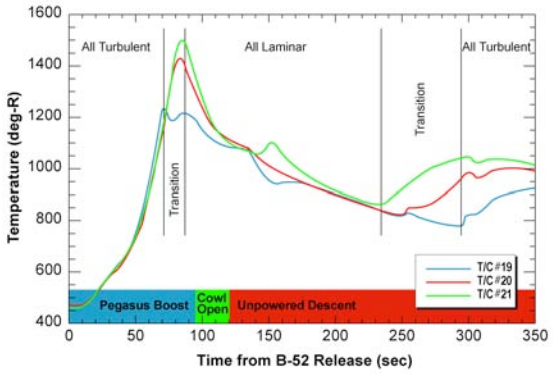

Figure 12. Flight 2 X-43A Upper Surface Temperatures from B-52 Drop to Splash

Figure 12 provides upper surface temperature time histories during the entire flight 2 trajectory from the point of release from the B-52. The three upper surface thermocouples (T/C) were evenly spaced along the vehicle centerline starting about midpoint for T/C#19 and ending near the trailing edge for T/C#21. Note that by the time the cowl opens and the scramjet is ignited, the entire upper surface appears to be laminar, as indicated by the dramatic temperature decrease that begins at about 70 seconds for the farthest forward T/C and 85 seconds for the farthest aft T/C. Likewise, at about 240 seconds the boundary layer transitions from laminar to turbulent as the vehicle decelerates. These results are discussed relative to pre-test predictions in detail in reference 34 along with discussions of the trip effectiveness on the lower surface.

Thermal Loads

Preliminary and continuing assessment of thermal loads for the F2 and F3, compared with design values, are documented in various sources[35-38]. These documents show that the engineering approach used in the design and development of the flight vehicles was generally conservative. However, some temperature measurements were higher than anticipated in regions of steep gradients, particularly late in the boost. The effect of "actual boost trajectory" vs. "design trajectory" is continuing to be studied. Results to date generally confirm prediction methods. Accuracy of the predictions appears significantly better than the assumed uncertainty for both Mach 7 and 10 flights. For example, figure 13 illustrates heating to the leading edge of the vehicle predicted using the "as flown" trajectory, with measured temperature within the C-C leading edge material. Adjacent nodes from the FEA model bracket the measured temperatures over the boost and scramjet-powered flight at Mach 10.

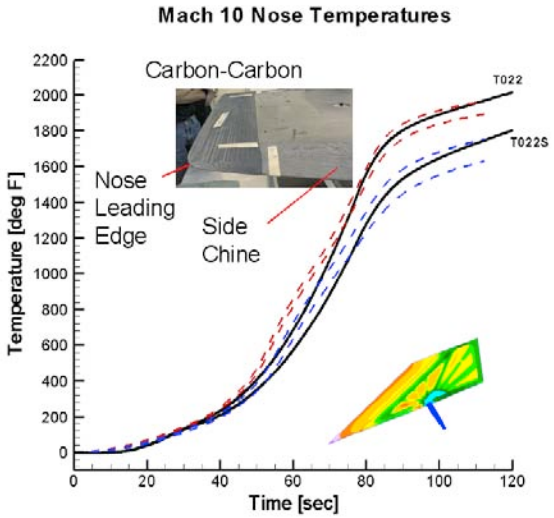

Figure 13. Flight 3 nose LE temperature confirms thermal model

Post Test Analysis

Posttest analysis of the flight data is underway at NASA Langley Research Center and elsewhere. This is required to model the "as flown" trajectory to properly assess thermal loads; to assess inlet mass capture at exactly the flight condition evaluated[39] using analytical methods; to evaluate the boundary layer state for BLT assessment; and to assess the overall vehicle drag, engine force, and vehicle acceleration/deceleration at exact flight conditions and control surface positions. Complete nose-to-tail CFD solutions for the actual flight condition are discussed in references 39 and 40. These solutions, for cowl closed, cowl open, and powered operation show excellent agreement (within a few percent) with measured acceleration/deceleration in flight (fig. 14). They also demonstrate the significant increase in computational throughput, which permit full 3-D solutions for the entire X-43A vehicle, which were not possible at earlier stages of the Hyper-X Program.

Another post-test analysis was to determine the engine Isp as tested, and "scale" to a vision vehicle, removing effects of small scale, cold fuel, fuel equivalence ratio, operating dynamic pressure, etc. This analysis is discussed in reference 41 and unclassified results shown in figure 15. The effective impulse developed in this scaling study will certainly set the standard for follow-on vehicle configurations.

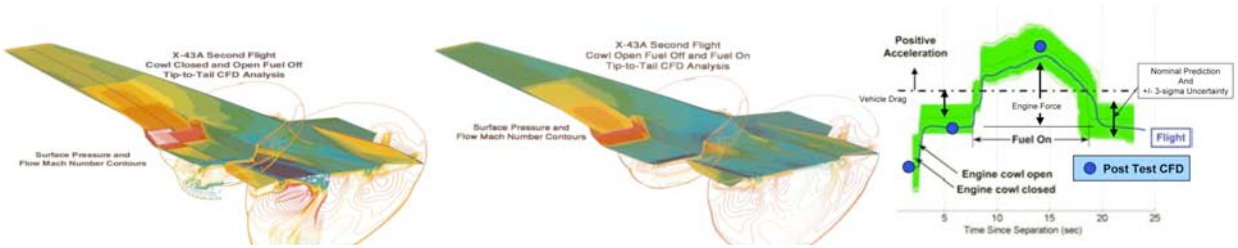

a). Unpowered; Cowl Closed and Open Tare *b) Fueled* *c) Comparison with Flight Acceleration*

Figure 14. Flight 2 X-43A Post Test CFD Solutions

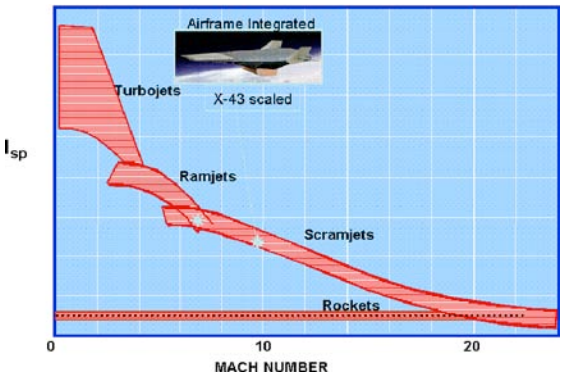

Figure 15. X-43A Isp Scaled to Vision Vehicle

SUMMARY AND CONCLUSIONS

The 2nd and 3rd flights of the X-43A were successfully completed on March 27 and November 16, 2004. This was the world's first scramjet-powered aircraft, and is recognized as the world's fastest "jet-powered aircraft." All phases of these two flights were performed as planned. The booster delivered the stack to the stage separation point at slightly lower Mach number and dynamic pressure than expected. The stage separation system performed smoothly, accomplishing the first known successful non-symmetric, high-dynamic pressure, high Mach number stage separation. Vehicle flight controls held angle of attack commanded to within a few tenths of a degree. Both vehicle drag and lift were slightly higher than predicted, but within the design uncertainty. The F2 vehicle accelerated under its own power for 15 miles in 11 seconds. The F3 vehicle demonstrated powered cruise at Mach 9.68, at 110,000 ft. altitude, covering 20 miles in 10.5 seconds of powered flight. Scramjet thrust measured matched prediction to within better than 2%. A significant, excellent-quality database was generated, which is only now starting to be evaluated. Analysis and validation of design methods are continuing, but the conclusion is clear: scramjet-powered vehicles can meet the performance claims and challenges of the next generation of air vehicles!

REFERENCES

1. H. Julian Allen: "Hypersonic Flight and the Re-entry Problem," The Twenty-First Wright Brothers Lecture. Journal of the Aerospace Sciences, Vol. 25, No. 4, April 1958.
2. Bilardo, V.J.; Hunt, J.L.; Lovell, N.T.; Maggio, G.; Wilhite, A.W.; and McKinney, L.E.: The Benefits of Hypersonic Airbreathing Launch Systems for Access to Space. AIAA 2003-5265. July 2003, Huntsville, AL.
3. McClinton, C.R.; Andrews, E.H; and Hunt, J.L.: Engine Development for Space Access: Past, Present and Future. 26th JANNAF Airbreathing Propulsion Subcommittee (APS) Meeting, Destin, FL April 8-12, 2001.
4. McClinton, C.R. and Rausch, V.L.: Hyper-X Program Status. 26th JANNAF Airbreathing Propulsion Subcommittee (APS) Meeting, Destin, FL April 8-12, 2002.
5. Storch, A.R.; Ferlemann, S.M; Bittner, R.D.: Hyper-X, Mach 7 Scramjet Preflight Predictions versus Flight Results. 28th JANNAF Airbreathing Propulsion Subcommittee Meeting. Charleston, SC. June 13-17, 2005.
6. Ferlemann, S.M.; Voland, R.T.; Cabell, K, Whitte, D.; and Ruf, E.: Hyper-X Mach 7 Scramjet Pretest Predictions and Ground to Flight Comparison. AIAA 2005-3322. Presented at 13th International Space Planes and Hypersonic Systems and Technology Conference, Capua, Italy. May 2005.
7. Ferlemann, P.: Hyper-X Mach 10 Scramjet Preflight Predictions vs. Flight Data. AIAA 2005-3352. Presented at 13th International Space Planes and Hypersonic Systems and Technology Conference, Capua, Italy. May 2005.
8. Redifer, M.E.; Lin, Y.; Kelly, J.; Hodge, M.; and Barklow, C.: The Hyper-X Flight System Validation Program. Hyper-X Program Office Report: HX-849. 2003. (also: Hyper-X Fluid/ Environmental Systems: Ground and Flight Operation and Lessons Learned. 28th JANNAF Airbreathing Propulsion Subcommittee Meeting. Charleston, SC. June 13-17, 2005.)
9. Harsha, P.T.; Keel, L.C.; Castrogiovanni, A.; and Sherrill, R.T.: X-43A Vehicle Design and Manufacture. 28th JANNAF Airbreathing Propulsion Subcommittee Meeting. Charleston, SC. June

13-17, 2005. (See also: Keel, L.C.: X-43A Research Vehicle Design and Manufacture. AIAA 2005-3334. Harsha, P.T.; Keel, L.C.; Castrogiovanni, A.; and Sherrill, R.T.: X-43A Vehicle Design and Manufacture. Presented at 13th International Space Planes and Hypersonic Systems and Technology Conference, Capua, Italy. May 2005.)

10. Keel, L.C.: X-43A Design and Manufacture (Mach 7 and 10). 28th JANNAF Airbreathing Propulsion Subcommittee Meeting. Charleston, SC. June 13-17, 2005.
11. Joyce, P.J.; Pomroy, J.B. and Grindle, L.: The Hyper-X Launch Vehicle: Challenges and Design Considerations for Hypersonic Flight Testing. AIAA 2005-3333, Presented at 13th International Space Planes and Hypersonic Systems and Technology Conference, Capua, Italy. May 2005.
12. Joyce, P.J.; and Pomroy, J.B.: Launch Vehicle Design Challenges for Hypersonic Flight Testing (Mach 7 and 10). 28th JANNAF Airbreathing Propulsion Subcommittee Meeting. Charleston, SC. June 13-17, 2005.
13. X-43A Mishap Investigation Board: Report of Findings: X-43A Mishap. NASA Washington, DC. May 8, 2003.
14. McClinton, C.R.; Rausch, V.L.; Nguyen, L.T.; and Sitz, J.R: "Preliminary X-43 Flight Test Results," IAC 04-V6-X42A 2, Nov. 2004.

14.1. McAllister, D.W.; Neal, B.A.; Dowdell, D.B.; McMullen, W. and Fullerton, G.: Hyper-X Flight 2 and 3 Ground and Flight Operations. 28th JANNAF Airbreathing Propulsion Subcommittee Meeting. Charleston, SC. June 13-17, 2005.

15. Corpening, G.; Marshall, L.; Sherrill, R.; and Nguyen, L.: A Chief Engineer's View of NASA's X-43A Scramjet Flight Test. AIAA 2005-3332. Presented at 13th International Space Planes and Hypersonic Systems and Technology Conference, Capua, Italy. May 2005.
16. Marshall, L.; Bahm, C.; Corpening, G.; and Sherrill, R.: X-43A Flight 3 Preparation and Results. AIAA 2005-3336. Presented at 13th International Space Planes and Hypersonic Systems and Technology Conference, Capua, Italy. May 2005.
17. Marshall, L.A.; Corpening, G.P.; Bahm, C.M; and Sherrill, R.T: A Chief Engineer's View of the NASA X-43A Flight 1, Flight 2, Flight 3, and Lessons Learned. 28th JANNAF Airbreathing Propulsion Subcommittee Meeting. Charleston, SC. June 13-17, 2005.
18. Morelli, E.A.; Derry, S.D.; and Smith, M.S.: "Aerodynamic Parameter Estimation for Flight 2 of the X-43A," Paper No. 20, Joint Army Navy NASA Air Force (JANNAF) Conference. Charleston, SC. June 2005.
19. Jones, T.P.; Rock, K.E.; Cabell, K.; Nugent, M.; and Miranda, L.: Flight Test Performance Summary of the Propulsion System Controller of the X-43A Vehicles. Presented at 28th Airbreathing Propulsion Subcommittee Meeting. Charleston, South Carolina. June 2005.
20. Del Corso, J.A.; and Hyper-X Staff: X-43A Flight 2 Data Release. HX-1076, NASA Langley Research Center, Hyper-X Program Office, March 2005.
21. Del Corso, J.A.; and Hyper-X Staff: X-43A Flight 3 Data Release. HX-1077, NASA Langley Research Center, Hyper-X Program Office, May 2005.
22. Karlgaard, C.D.; Tartabini, P.V. and Toniolo, M.D.: Hyper-X Post–Flight Trajectory Reconstruction. AIAA Atmospheric Flight Mechanics Conference and Exhibit. AIAA 2004-4829, Aug. 2004. (also: Karlgaard, C.; and Tartabini, P.V.: Best Estimated Trajectory Reconstruction for the X-43A Mach 7 and 10 Flights. 28th JANNAF Airbreathing Propulsion Subcommittee Meeting. Charleston, SC. June 13-17, 2005.)
23. Vause, R.F.; Moore, D.F.; and Risner, N.: Weight Reduction Studies for the Hyper-X Mach 10 Vehicle. 28th JANNAF Airbreathing Propulsion Subcommittee Meeting. Charleston, SC. June 13-17, 2005.
24. Baumann, E.A.: X-43A Guidance, Navigation and Control Challenges (Mach 7 and 10). 28th JANNAF Airbreathing Propulsion Subcommittee Meeting. Charleston, SC. June 13-17, 2005. (Also: Bahm, C.; Strovers, B.; Baumann, E.; Beck, R.; Bose, D.: X-43A Guidance, Navigation and Control Challenges. AIAA-2005-3275. Presented at 13th International Space Planes and Hypersonic Systems and Technology Conference, Capua, Italy. May 2005.)
25. Martin, J.G.; Reubush, R.E; and Bose, D.M.: Hyper-X Stage Separation. 28th JANNAF Airbreathing Propulsion Subcommittee Meeting. Charleston, SC. June 13-17, 2005.
26. Tartabini, P.V.; Martin, J.G.; Bose, D.M.; Thornblom, M; and Lien, J.P.: Mach 10 Stage Separation Analysis for the X-43A. 28th JANNAF Airbreathing Propulsion Subcommittee Meeting. Charleston, SC. June 13-17, 2005.
27. Blocker, W.: and Reubush, D.E.: X-43A Stage Separation System—A Flight Data Evaluation. AIAA 2005-3335. Presented at 13th International Space Planes and Hypersonic Systems and Technology Conference, Capua, Italy. May 2005.
28. Engelund, W.C.: Hyper-X/X-43A Aerodynamics: Results from the Mach 7 and Mach 10 Scramjet Flight Test. 28th JANNAF Airbreathing Propulsion Subcommittee Meeting. Charleston, SC. June 13-17, 2005.
29. Engelund, W.C.: Hyper-X/X-43A Aerodynamics: Results from the Mach 7 and Mach 10 Scramjet Flight Test. AIAA 2005-3405. Presented at 13th International Space Planes and Hypersonic Systems and Technology Conference, Capua, Italy. May 2005.
30. Special Section: Hyper-X. *J. Spacecraft and Rockets*. Vol. 38, No. 6, Pg. 801-853. Nov-Dec. '01.

31. Ferlemann, P.G.: Comparison of Hyper-X Mach 10 Scramjet Predictions and Flight. 28th JANNAF Airbreathing Propulsion Subcommittee Meeting. Charleston, SC. June 13-17, 2005.
32. Ruf, E.G.; Cabell, D.W.; Witte, D.W.; and Shih, A.T.: Hyper-X Mach 7 Scramjet Ground to Flight Comparisons. 28th JANNAF Airbreathing Propulsion Subcommittee Meeting. Charleston, SC. June 13-17, 2005.
33. Rogers, R.C.; Shih, A.T.; and Hass, N.E.: Hyper-X Mach 10 Engine Flowpath Testing: Ground to Flight Comparisons. 28th JANNAF Airbreathing Propulsion Subcommittee Meeting. Charleston, SC. June 13-17, 2005.
34. Berry, S.A.; Daryabeigi, K.; Auslender, A.H. and Bittner, R.D: Boundary Layer Transition on the X-43A Flight 2. 28th JANNAF Airbreathing Propulsion Subcommittee Meeting. Charleston, SC. June 13-17, 2005.
35. Amundsen, R.M.; Leonard, C.P.; and Bruce, W.E. III: Hyper-X Hot Structures Comparison of Thermal Analysis and Flight Data. 15th Thermal and Fluids Analysis Workshop, Pasadena, CA. Aug. 30, 2004.
36. Leonard, C.P.; Bruce, W.; and Amundsen, R.M.: Hyper-X Hot Structures Design and Comparison with Flight Data. 28th JANNAF Airbreathing Propulsion Subcommittee Meeting. Charleston, SC. June 13-17, 2005.
37. Cuda, V.; and Woelfel, R.: Comparison of Hyper-X Engine Thermal Analysis and Flight Data. 28th JANNAF Airbreathing Propulsion Subcommittee Meeting. Charleston, SC. June 13-17, 2005.
38. Leonard, C.; Amundsen, R.; and Bruce, W.: Hyper-X Hot Structures Design and Comparison with Flight Data. AIAA 2005-3438. Presented at 13th International Space Planes and Hypersonic Systems and Technology Conference, Capua, Italy. May 2005.
39. Jentink, T.N. and Ferlemann, P.G.: Mach 10 Tip-to-Tail Preflight Prediction, 28th JANNAF Airbreathing Propulsion Subcommittee Meeting. Charleston, SC. June 13-17, 2005.
40. Meyer, B.M.: Tip to Tail Preflight Prediction. 28th JANNAF Airbreathing Propulsion Subcommittee Meeting. Charleston, SC. June 13-17, 2005.
41. Rock, K.E.; Voland, R.T.; and Witte, D.W.: Hyper-X Mach 7 and 10 Scramjet Operation. 28th JANNAF Airbreathing Propulsion Subcommittee Meeting. Charleston, SC. June 13-17, 2005.